Clim Dyn (2015) 44:2369–2382
DOI 10.1007/s00382-015-2476-6

Simulation of the South American climate by a coupled model with super-parameterized convection

V. Krishnamurthy · Cristiana Stan

Received: 19 December 2013 / Accepted: 7 January 2015 / Published online: 20 January 2015

Abstract The simulation of the climate over South America by a coupled ocean–atmosphere model with embedded cloud resolving model is studied on different time scales. The mean climate and the variability over South America as simulated by the superparameterized Community Climate System Model version 3 (SP-CCSM) are compared with those in the observation and in the control simulation of the CCSM3 (CT-CCSM) which employs conventional scheme of convection parameterization. The CT-CCSM is able to simulate only the longer period seasonal oscillation (SO) while the SP-CCSM is successful in simulating both the SO and the intraseasonal oscillation (ISO). The spatial structure and the propagation of the oscillations are better in the SP-CCSM. Both models are able to simulate the observed low-frequency modes of variability related to El Niño-Southern oscillation (ENSO) and Pacific decadal oscillation (PDO). While the ENSO mode in the CT-CCSM has more regular variability with a biennial time scale, the SP-CCSM simulates the ENSO mode with more irregular variability and time scale closer to the observation. The spatial structure, the relation with the Pacific and the regional variations of the observed PDO mode are better simulated by the SP-CCSM than the CT-CCSM.

V. Krishnamurthy (✉) · C. Stan
Center for Ocean-Land-Atmosphere Studies, Research Hall, MS 6C5, George Mason University, 4400 University Drive, Fairfax, VA 22030, USA
e-mail: krishna@cola.iges.org

C. Stan
Department of Atmospheric, Oceanic and Earth Sciences, George Mason University, Fairfax, VA, USA

1 Introduction

The climate over South America displays certain characteristics of monsoon systems which respond to seasonal development of land–ocean thermal contrast. The South American climate exhibits seasonal changes in precipitation, reversal of anomalous low-level winds and upper level anticyclone (Zhou and Lau 1998; Nogués-Paegle et al. 2002; Vera et al. 2006; Marengo et al. 2012). The austral seasonal convective heating over the Amazon and central Brazil induces Bolivian High and Nordeste Low in the circulation while the low-level easterlies from the Atlantic Ocean are steered by the Andes to the Chaco Low (Lenters and Cook 1997; Zhou and Lau 1998; Grimm et al. 2005). The precipitation and cloudiness from the Amazon to southeast Brazil extend into the Atlantic Ocean to form the South Atlantic Convergence Zone (SACZ).

The South American climate reveals strong variability on intraseasonal, interannual and interdecadal time scales (Nogués-Paegle et al. 2002; Vera et al. 2006; Marengo et al. 2012). The intraseasonal variability over South America involves a dipole pattern of wet and dry conditions alternating over the SACZ and the subtropical plains (Nogués-Paegle and Mo 1997; Liebmann et al. 1999; Carvalho et al. 2002a, b; Jones and Carvalho 2002). This pattern was shown to be an intraseasonal oscillation propagating northeastward (Krishnamurthy and Misra 2011), and a relation with the Madden–Julian oscillation (MJO; e.g., Madden and Julian 1994) was also indicated (Carvalho et al. 2004; Liebmann et al. 2004; Krishnamurthy and Misra 2011). In the same region, another propagating oscillation with a dipole pattern and a period of about 5.5 months exists and shows teleconnection with the North Atlantic oscillation (NAO) (Krishnamurthy and Misra 2011).

On the interannual time scale, the El Niño-Southern oscillation (ENSO) has significant impact on the variability of rainfall during austral spring and summer seasons in the Amazon Basin (Kousky et al. 1984; Aceituno 1988; Ropelewski and Halpert 1987; Marengo 1992, 1995; Rao et al. 1996; Fu et al. 2001) and other regions (Silva and Ambrizzi 2006; Silva et al. 2009). During an El Niño (La Niña) year, the rainfall over the Amazon Basin is reduced (increased). Some studies have suggested that ENSO's influence on precipitation in southeast Brazil is subseasonal rather than on interannual time scale (Liebmann et al. 2001; Carvalho et al. 2002a). On the other hand, recent studies by Krishnamurthy and Misra (2010, 2011) have shown that ENSO is associated with seasonally persisting signal in central-east South America which varies on interannual time scale. The precipitation over South America also shows interdecadal variability associated with the Atlantic multidecadal oscillation (AMO) and the Pacific decadal oscillation (PDO) which can modulate the interannual variability of seasonal mean precipitation (Krishnamurthy and Misra 2011; Silva et al. 2011).

The prediction and simulation of the mean and variability of South American climate by models have met with varying degrees of success (Vera et al. 2006; Marengo et al. 2012). While some large-scale fields may be better simulated, the prediction of precipitation on seasonal to interannual time scales has been rather difficult. In an analysis of the simulation of the precipitation by coupled model intercomparison project phase 3 (CMIP3), Bombardi and Carvalho (2009) found that most models exhibited poor simulation of precipitation over the Amazon and northeastern Brazil although certain aspects of the annual cycle over central and eastern Brazil were better simulated. The importance of air-sea interaction in the ENSO teleconnection over the Amazon and, in general, over the global monsoon regions has been pointed out by Misra (2008a, b) in coupled model studies. Models also have considerable problem in properly simulating the MJO (Lin et al. 2006). Another important physical process that determines the variability over South America is convection. Most models treat convection and cloud formation through parameterization which leads to large systematic errors in climate simulations (Randall et al. 2007; Guilyardi et al. 2009). Explicit representation of the physical processes is still not possible because of the insufficient horizontal resolution of the present coupled models.

A multi-scale modeling framework (MMF) has offered a solution to explicitly treat convection by embedding high-resolution cloud resolving model (CRM) in a coarse-grid general circulation model (GCM) of large-scale circulation (Grabowski 2001; Khairoutdinov and Randall 2001). The embedding of CRM is also referred to as super-parameterization (SP) of small-scale processes. In a recent study, Stan et al. (2010) embedded two-dimensional CRMs in the Community Climate System Model (CCSM) of National Center for Atmosphere Research (NCAR) and demonstrated improved simulation of phenomena such as ENSO and MJO when compared to CCSM with conventional parameterization of convection. The superparameterized CCSM (SP-CCSM) indicated the necessity of coupled models as well as realistic convection parameterizations. The simulations of intraseasonal oscillations, interannual variability and propagation of equatorial waves in the South Asian monsoon region by SP-CCSM are shown to be better than those by either the CCSM with conventional parameterization or the super-parameterized atmospheric GCM (DeMott et al. 2011, 2013; Krishnamurthy et al. 2013).

The objective of this study is to investigate the ability of SP-CCSM to realistically simulate the mean conditions and variability on different time scales in the South American region. Specifically, the simulation of the observed intraseasonal and interseasonal oscillations, interannual and interdecadal modes in the South American climate (Krishnamurthy and Misra 2010, 2011) by the SP-CCSM will be examined. The impact of using CRMs is assessed by comparing the simulations of SP-CCSM and CCSM with convectional parameterization.

In Sect. 2, the observed data, model simulations and the methodology are described. Section 3 discusses the mean monsoon and the different modes of variability. The intraseasonal and interseasonal oscillations are described in Sect. 4 while low-frequency modes are discussed in Sect. 5. Summary and conclusions are provided in Sect. 6.

2 Models, data and method of analysis

2.1 Models and data

The coupled model used in this study is the NCAR CCSM version 3 (Collins et al. 2006) which has Community Atmospheric Model version 3 (CAM3) with T42 horizontal resolution as the atmospheric component while the ocean component is the low-resolution (3.6° in longitude and varying in latitude) Parallel Ocean Program (POP) model. The CCSM uses the conventional parameterization of deep convection by Zhang and McFarlane (1995). The two-dimensional CRM used for SP and its embedding in CAM are described by Khairoutdinov and Randall (2001, 2003), and the incorporation of SP in CCSM was carried out by Stan et al. (2010). The domain of the CRM is aligned in the East–West direction, and the horizontal resolution is 4 km. The present study has analyzed a 20-year long simulation by SP-CCSM and compared with a similar control simulation by CCSM (CT-CCSM) using conventional parameterization. For this purpose, daily mean values of outgoing longwave radiation (OLR), 850 hPa

horizontal wind, sea surface temperature (SST) and mean sea level pressure (MSLP) have been analyzed.

The observed daily mean OLR data used in this study were obtained from the National Oceanic and Atmospheric Administration (NOAA; Liebmann and Smith 1996) on 2.5° × 2.5° grid for the period 1984–2003. Daily means of zonal wind u, meridional wind v and MSLP from the ERA-Interim reanalysis of the European Centre for Medium Range Forecasts (Dee et al. 2011) on T255 horizontal grid for 1984–2003 were used. From the Optimally Interpolated SST version 2 (OISST2) dataset developed by NOAA (Reynolds et al. 2007), daily averages of SST on 0.25° × 0.25° grid were obtained for the period 1984–2003. Daily climatology has been removed from the daily means to obtain daily anomalies for all the observed and model data. For convenience, in the rest of the paper, observations refer to all the data products (including reanalysis) used for the model evaluations.

2.2 Method of analysis

The space–time modes of South American climate are obtained by applying the multichannel singular spectrum analysis (MSSA) which is a data-adaptive method that can extract nonlinear oscillations, persistent modes and trends from the time series of spatial data (Ghil et al. 2002). Although MSSA is equivalent to the extended empirical orthogonal function analysis, it has undergone more refinement in nonlinear dynamical systems theory, and differs in the choice of key parameters such as the width of the lag window and in the interpretation of the results (Ghil et al. 2002). In MSSA, a given time series $X(t)$ at L grid points (channels), where time $t = 1, 2, 3\ldots N$, is augmented with M lagged copies of the time series to construct a grand lag-covariance matrix C. When C is diagonalized, the result consists of LM eigenvalues and LM eigenvectors which are the space–time empirical orthogonal functions (ST-EOFs). The corresponding space–time principal components (ST-PCs) are obtained by projecting the original time series on the ST-EOFs. The reconstructed component (RC) of a particular eigenmode is constructed by combining the corresponding ST-EOF and ST-PC (see Ghil et al. 2002, for the formula). The RCs have the same time and space dimensions and the phase of the original time series. A pair of eigenmodes having nearly equal eigenvalues and periods with their ST-EOFs and ST-PCs in quadrature is identified as an oscillation (Plaut and Vautard 1994).

3 Mean climate and modes of variability

3.1 Mean and standard deviation

Before discussing the modes of variability over South America, a brief description of the mean climate and standard deviation is provided. The spatial structures of December–March (DJFM) seasonal climatological means of OLR, 850 hPa horizontal wind and SST in the model simulations are compared with observations. Similar comparison is also made for the standard deviations of daily anomalies of the three fields for the DJFM season. The climatology and standard deviation in the observation are computed for the period 1984–2003 while 20-year simulations are used in the case of the models. The observed mean OLR (Fig. 1a) indicates strong convection over a large area north of 20°S, which includes the Amazon River Basin, while moderate convection is seen over the southern part of the continent and SPCZ and weaker convective activity over the equatorial Pacific and Atlantic oceans. The observed spatial structure of the mean OLR is reasonably well simulated by both CT-CCSM (Fig. 1b) and SP-CCSM (Fig. 1c). However, there are some regional deficiencies such as higher OLR values (lesser convection) in the oceanic regions, eastern Brazil and in the core monsoon region. While the simulation of the strong convection in the northern part of the continent is better in CT-CCSM compared to SP-CCSM, the mean OLR over the oceanic

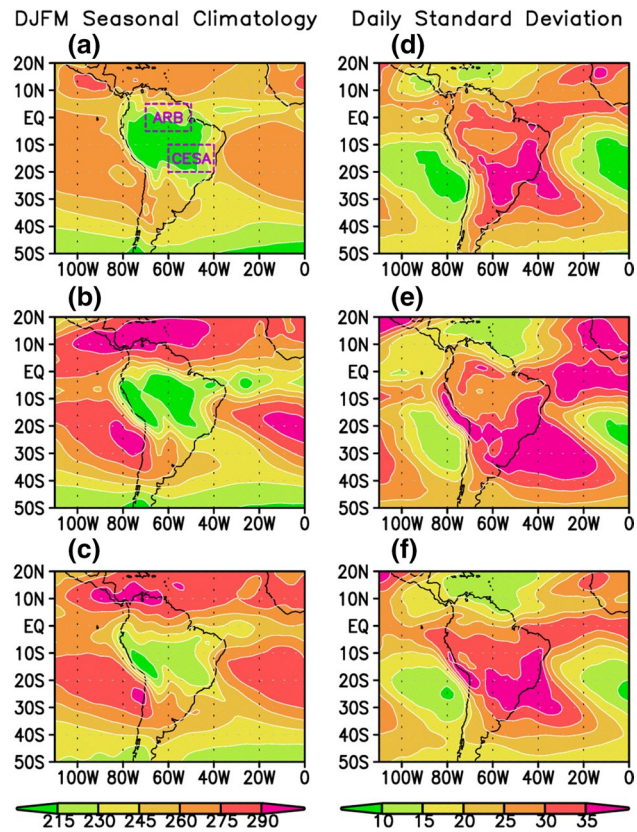

Fig. 1 DJFM seasonal climatological mean of OLR in **a** observation, **b** CT-CCSM and **c** SP-CCSM. Standard deviation of daily mean OLR for DJFM season in **d** observation, **e** CT-CCSM and **f** SP-CCSM. Units are in W m^{-2}

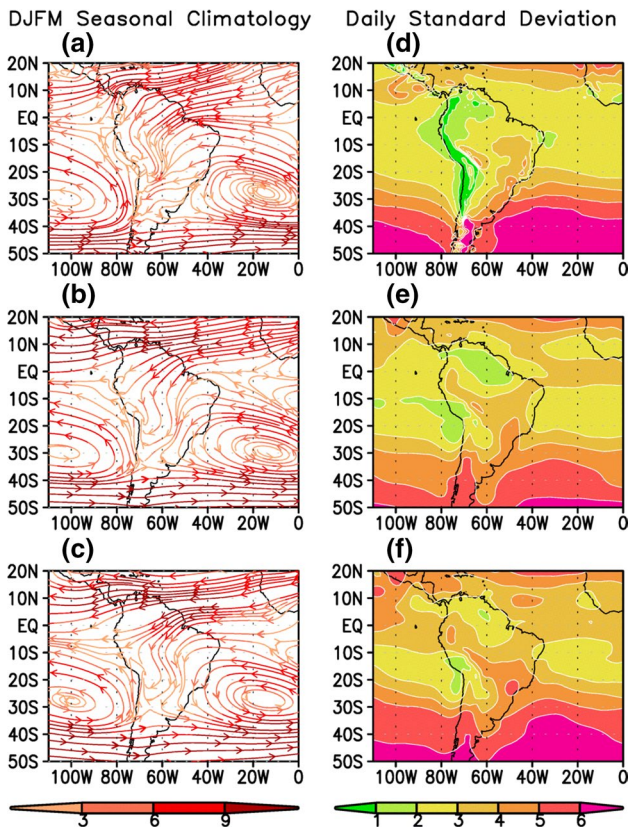

Fig. 2 DJFM seasonal climatological mean of 850 hPa horizontal wind (*streamlines*) in **a** observation, **b** CT-CCSM and **c** SP-CCSM. Standard deviation of daily mean 850 hPa zonal wind for DJFM season in **d** observation, **e** CT-CCSM and **f** SP-CCSM. Units are in m s^{-1}

regions is better simulated by SP-CCSM. The DJFM climatological mean of 850 hPa horizontal wind in observation (Fig. 2a) is well simulated by both CT-CCSM (Fig. 2b) and SP-CCSM (Fig. 2c) which capture the northeasterly flow from the Atlantic in the equatorial region, anticyclonic flows in the subtropical Pacific and Atlantic oceans, and the westerly flow in the south. However, both models are deficient in reproducing the observed low-level jet east of the Andes, perhaps because of low horizontal resolution in the boundary conditions. The observed DJFM climatological mean SST (Fig. 3a) is reasonably well simulated by CT-CCSM (Fig. 3b) and SP-CCSM (Fig. 3c). However, lesser meridional extent of warm SST in the West Pacific and colder SST along equatorial eastern coast of the continent are seen in both models.

The standard deviation of daily OLR for DJFM season in the observation (Fig. 1d) is in the range of 25–40 W m^{-2} over most of the continent with a maximum in the SACZ while there are regions of minimum in the Pacific and Atlantic oceans. The SP-CCSM (Fig. 1f) has simulated the structure and magnitude of the standard deviation close to the observation except for slightly higher values in the oceanic regions of minima whereas the CT-CCSM simulation (Fig. 1e) has higher values over most of the domain. The standard deviation of daily zonal wind at 850 hPa for DJFM in the observation is nearly uniform (2–4 W m^{-2}) in the tropics except for lower values along the west coast and increases southward (Fig. 2d). Both CT-CCSM (Fig. 2e) and SP-CCSM (Fig. 2f) show slightly higher values in the tropics but fail to capture the lower values along west coast and the Andes as in case of the climatological mean of the horizontal wind. The SP-CCSM is closer to the observation than CT-CCSM in the southern region. The standard deviation of daily SST for DJFM is about 0.2–0.6 °C over most of the Atlantic in the observation (Fig. 3d) while it is slightly lower in both CT-CCSM (Fig. 3e) and SP-CCSM (Fig. 3f). The observed ENSO signature in the Pacific (Fig. 3d) is also simulated by both CT-CCSM and SP-CCSM (Fig. 3e, f) but with some slight differences. The region of maximum SST anomaly (>1 °C) along the equator is extended in zonal and meridional directions in CT-CCSM whereas it is somewhat closer to the observed structure in SP-CCSM. Both models show slightly less activity away from the equator.

3.2 MSSA modes

The space–time modes of convection over South America were obtained by applying MSSA on daily OLR anomalies in the (110°W–0°, 50°S–20°N) domain. This analysis was performed separately for observation and simulations of CT-CCSM and SP-CCSM. In order to extract the oscillation of longer period also, the MSSA was applied on the anomalies of all the days of the data period using a lag window of 241 days at 1 day interval. In each case, the ST-EOFs and ST-PCs of the MSSA eigenmodes were examined to identify the persistent and oscillatory modes. A pair of eigenmodes with nearly equal eigenvalues and in quadrature forms an oscillation (Plaut and Vautard 1994). The RCs were constructed for the persisting modes and oscillations following the method by Gill et al. (2002).

In the observed OLR, the first three MSSA eigenmodes were found to be persistent modes while two oscillatory pairs emerged from the next four eigenmodes, similar to the eigenmodes obtained by Krishnamurthy and Misra (2011). The variance explained by these modes ranges from 0.9 to 0.3 % of the total variance. These small values are typical of MSSA eigenmodes of raw daily anomalies without applying any pre-filter. Consistent with the study by Krishnamurthy and Misra (2011), the three persisting modes are related to ENSO, AMO and PDO, and the two oscillatory pairs have broad-band spectra with peaks centered at 165 and 52 days. To use distinct abbreviations, the longer period oscillation will be referred to as seasonal

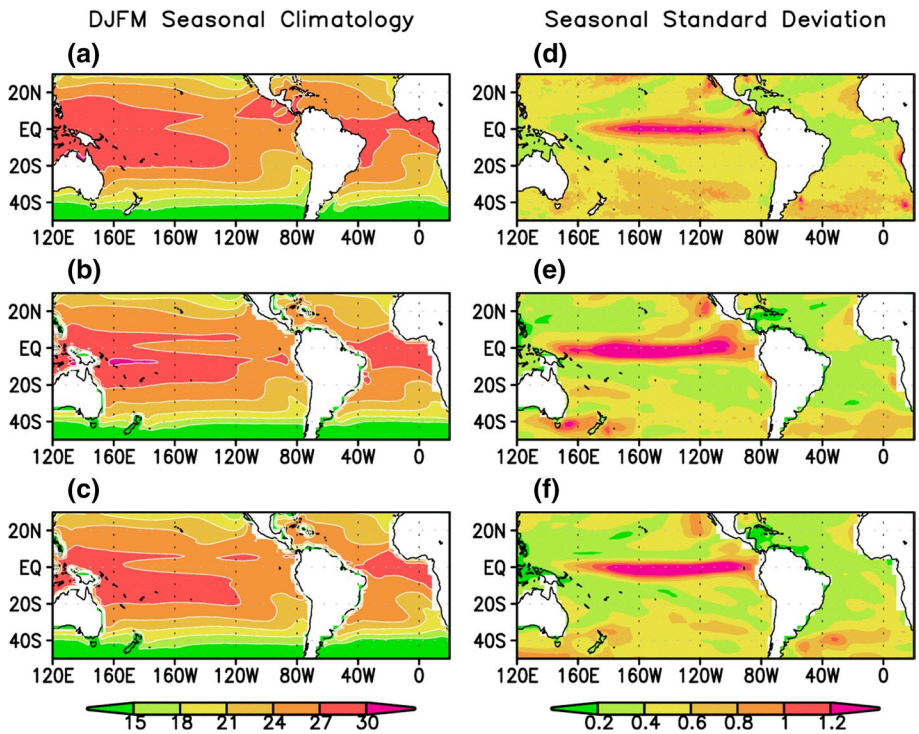

Fig. 3 DJFM seasonal climatological mean of SST in **a** observation, **b** CT-CCSM and **c** SP-CCSM. Standard deviation of DJFM seasonal mean of SST in **d** observation, **e** CT-CCSM and **f** SP-CCSM. Units are in °C

oscillation (SO) while the shorter period oscillation will be called as intraseasonal oscillation (ISO). The SO is the same as the interseasonal oscillation related to NAO in the study by Krishnamurthy and Misra (2011) and the ISO is associated with the MJO.

An examination of the MSSA eigenmodes of CT-CCSM and SP-CCSM showed the presence of persisting modes related to ENSO and PDO in both the models. However, the persisting mode associated with AMO was not found in either model. While the SP-CCSM revealed the existence of both SO and ISO, the CT-CCSM showed the presence of SO only. The variance explained by each mode in the models is very close to the variance of the corresponding mode in the observation. In the next two sections, the oscillations and the persisting modes found in CT-CCSM and SP-CCSM will be compared with the corresponding modes in the observation. The analysis will examine whether the SP-CCSM is better than CT-CCSM in simulating the various modes.

4 Oscillatory modes

In this section, the oscillatory modes obtained from the MSSA of daily OLR anomalies in the observation and model simulations are described. For further examination, a spatial EOF analysis of the RC of each oscillation was performed. Almost all the variance of each RC is explained by its first two spatial EOFs (S-EOFs), and the first two spatial PCs (S-PCs) are in quadrature. The power spectra of the first S-PC (S-PC1) of the RCs of SO and ISO in the observation, shown in Fig. 4a, are broad-band with peaks at 165 and 56 days, respectively. The CT-CCSM simulation reveals only SO, and the power spectrum of the S-PC1 of its RC shows a peak at 138 days (Fig. 4b), lower than the observed period. The SP-CCSM is able to simulate both SO and ISO. The power spectrum (Fig. 4c) of the S-PC1 of the RC of SO in SP-CCSM has a peak at 203 days which is higher than the observed period while the ISO shows a spectral peak at 46 days which is slightly lower than the observed period.

To study the space–time evolution of each oscillation, the amplitude $A(t)$ and phase $\theta(t)$ of the oscillation at time t are determined from the S-PC1 of the RC following the method suggested by Moron et al. (1998). The composites of RC or any other field based on the phases of the oscillation provide the space–time evolution. The phase composites are constructed by averaging the RC in eight equal intervals of $\theta(t)$ between 0 and 2π for the entire period of the analysis.

4.1 SO

The evolution of the SO is shown by the phase composites of the OLR RC in Fig. 5 for the first half cycle of the oscillation in observation, CT-CCSM and SP-CCSM. The average period of a complete cycle of SO is 165, 138 and 203 days in observation, CT-CCSM and SP-CCSM,

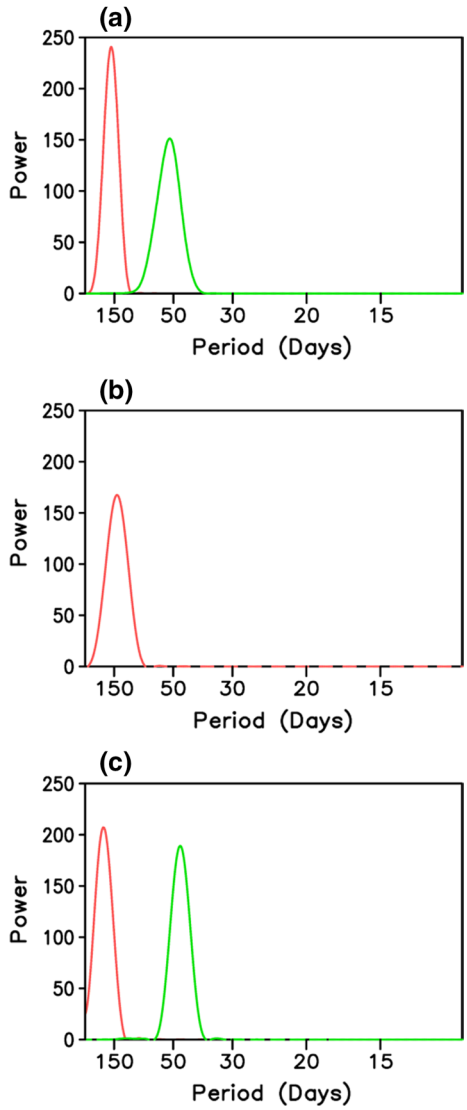

Fig. 4 Power spectra (in units of day^{-1}) of the S-PC1 of the RCs of SO (*red*) and ISO (*green*) in **a** observation, **b** CT-CCSM and **c** SP-CCSM

respectively. In the observation (Fig. 5a), anomalies of convection appear over the SACZ region in phase 1. The convective anomalies become more intense and propagate northeastward in phases 2–3 and eventually diminish in phase 4. Areas of suppressed convection are seen in the northern region during phases 1–3. The same sequence occurs during phases 5–8 with anomalies of opposite sign (figure not shown).

The phase composites in CT-CCSM (Fig. 5b) show that convective anomalies, which develop around 20°S in phase 1, intensify and cover almost the entire northern part of the continent in phases 2–3. These anomalies extend farther south over the ocean in SACZ than in the observation. The convective anomalies are still stronger and cover a larger region in phase 4. The northeastern movement is slower in CT-CCSM compared to the observation. Stronger positive anomalies representing suppressed convection exist over the equatorial Atlantic in phases 1–3, unlike in the observation. The SP-CCSM also reveals northeastward propagating convective anomalies in the phase composites (Fig. 5c). In phases 1–2, the convective anomalies are somewhat similar to those in the observation but less intense in phase 3. The northeastward movement is more obvious in phase 4 than in CT-CCSM. The positive anomalies in the northern part of continent and the equatorial Atlantic are comparable to those in the observation. The SP-CCSM, however, shows stronger than observed positive anomalies in a small region of the equatorial Pacific and a spurious convective band of precipitation across South America from SACZ to the equatorial Pacific.

A possible association between SO and NAO in the observation was suggested by Krishnamurthy and Misra (2011). To test whether a similar relation is also exhibited by the model simulations, the phase composites of MSLP and 1,000 hPa zonal wind u corresponding to SO were examined. For brevity, the phase composites are shown in Fig. 6 only for the peak phase of SO (phase 3). The MSLP composite in SP-CCSM (Fig. 6b) shows low pressure in the region 40°N–60°N and high pressure to the north of 60°N associated with the convective anomalies of SO. The 1,000 hPa zonal wind composite associated with this pressure pattern in SP-CCSM has easterlies in the southern part and westerlies in the northern part of the region (Fig. 6d). Both the MSLP and zonal wind composites have good correspondence with the observed structure shown by Krishnamurthy and Misra (2011; Fig. 11). The MSLP composite in CT-CCSM, however, is less intense and is shifted southward by about 20° (Fig. 6a). The associated composite of 1,000 hPa zonal wind in CT-CCSM (Fig. 6c) shows weaker anomalies of opposite sign compared to the composites of SP-CCSM and observation.

4.2 ISO

As discussed earlier, the ISO is simulated by SP-CCSM while the CT-CCSM is not able to resolve this oscillation. The space–time structure of ISO in the observation and SP-CCSM is studied by the phase composites of the respective RC of the ISO. The phase composites of the RCs shown in Fig. 7 depict the first half cycle of the ISO in the observation and SP-CCSM. The average period of one complete cycle of ISO in SP-CCSM is 46 days, which is slightly less than the observed period of 52 days.

In the observation (Fig. 7a), phase 1 shows convective anomalies around 20°S aligned along the SACZ and also in the equatorial Pacific. These anomalies intensify and expand toward the northwest region of the continent

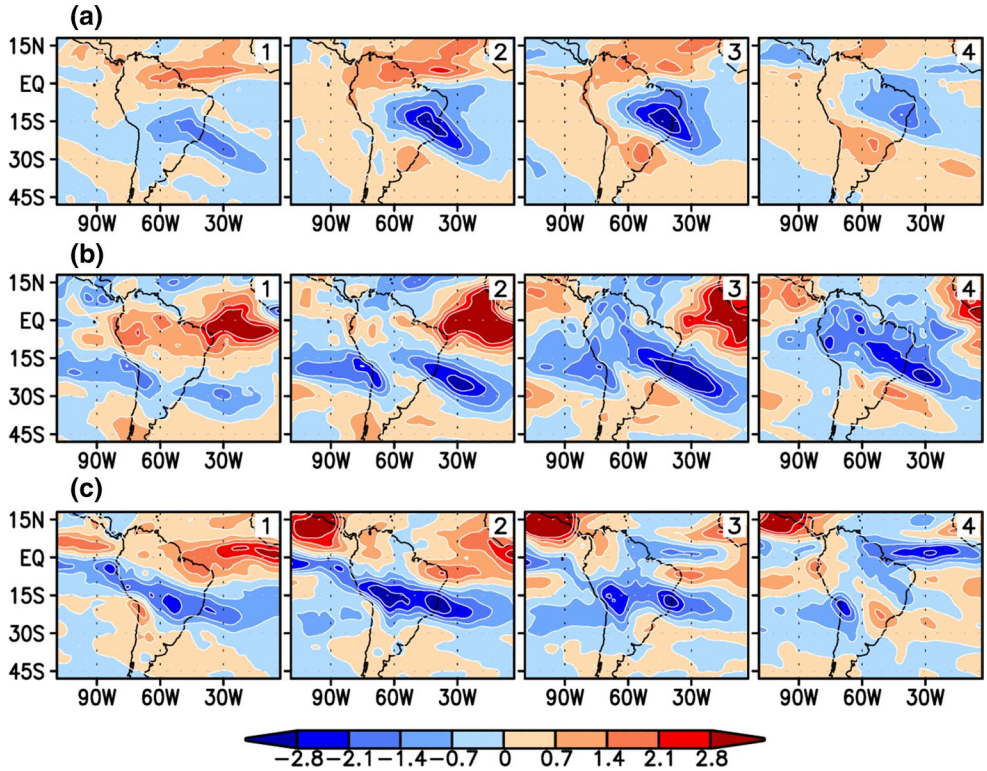

Fig. 5 Phase composites of the OLR RCs for four phase intervals of an average cycle of SO in **a** observation, **b** CT-CCSM and **c** SP-CCSM. Each phase interval is of length π/4 and the *phase number* is given at the *top right* corner of each panel. Units are in W m^{-2}

in phases 2 and 3. The convective anomalies form a large tilted band from the equatorial Pacific to the oceanic region of SACZ and propagate northeastward. In phase 4, the convective activity weakens and moves further northeastward. In phases 2–4, the positive anomalies from the previous cycle move further north in the equatorial Atlantic and northern part of the continent. During phases 1–4, new suppressed convection anomalies develop in the southern part of the continent and move northeastward. These positive anomalies go through the same sequence in phases 5–8 (figure not shown), similar to phases 1–4 but with anomalies of opposite sign.

The phase composites of the RC of ISO in SP-CCSM (Fig. 7b) have reasonably good resemblance to the observed cycle (Fig. 7a). The spatial structure and the northeastward propagation of the convective anomalies are captured by the SP-CCSM. However, in all the four phases, the convective anomalies are weaker in SP-CCSM compared to observation. The convective anomalies extend from the equatorial Pacific to the SACZ region during phases 2–3, at a slower speed than in observations. The positive anomalies from the previous cycle are stronger over the equatorial Atlantic and continue to move northeastward instead of northward as in the observation. As shown by Krishnamurthy and Misra (2011), the time variability of the ISO consists of stronger amplitudes during austral summer and weaker amplitudes during austral winter (see their Fig. 3e). The SP-CCSM model also captures the seasonal variation of the amplitude of the ISO (figure not shown). Observational evidence provided by Krishnamurthy and Misra (2011) suggested that the ISO is associated with the MJO. The SP-CCSM was shown to better simulate the MJO and its propagation by Stan et al. (2010). Whether the SP-CCSM also captures the ISO-MJO relation is tested by examining the ISO phase composites of the total OLR anomalies in the tropical region. As shown in Fig. 8, the first half cycle of the phase composites of the OLR anomalies reveals convective anomalies propagating eastward from the Maritime Continent to the equatorial central Pacific in phases 1–4. In association, the propagation of the ISO over the South American continent and the Atlantic is also evident in the total OLR anomalies (Fig. 8), similar to the propagation of the RC of the ISO (Fig. 7b). Thus, the SP-CCSM is also able to relate the ISO with the propagation of the MJO in the model.

5 Low-frequency modes

The low-frequency modes, which were obtained as seasonally persisting modes in the MSSA, are discussed in this section. As described in Sect. 3.2, the low-frequency modes in the observation correspond to the modes found by Krishnamurthy and Misra (2011) and related to ENSO, AMO and PDO. The MSSA of CT-CCSM and SP-CCSM simulations revealed low-frequency modes related to

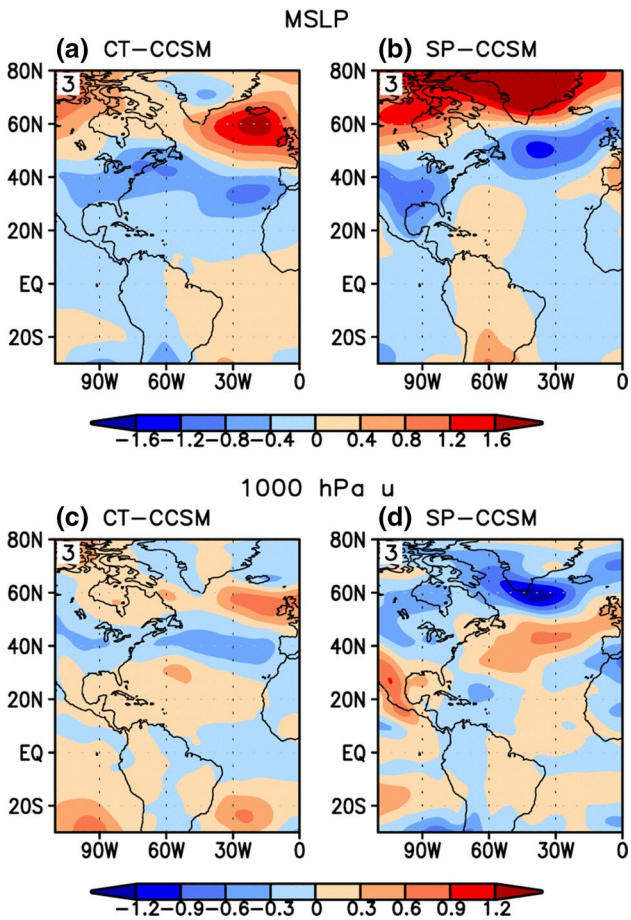

Fig. 6 Phase composites of daily MSLP anomalies in **a** CT-CCSM and **b** SP-CCSM and phase composites of 1,000 hPa zonal wind anomalies in **c** CT-CCSM and **d** SP-CCSM for the peak phase interval 3 in SO. Units are in hPa for MSLP and m s^{-1} for the zonal wind

ENSO and PDO but not the AMO mode. The rest of this section will discuss the ENSO and PDO modes in the models and compare with the corresponding modes in the observation.

5.1 ENSO and PDO modes

The low-frequency modes in the model simulations and observation were identified by performing spatial EOF analysis of the RCs of the MSSA eigenmodes. Since these are coherent modes, the first EOF of the RC explains almost all of the variance of the RC. The power spectrum of the S-PC1 of the RC in each case is plotted in Fig. 9. In the observation, the ENSO mode shows a broad-band spectrum with a peak at 48 months while the PDO mode shows a red spectrum in the time period of the analysis because of its longer period (Fig. 9a). The spectra of the CT-SSCM simulation (Fig. 9b) reveal a broad-band spectrum with a peak at 26 months for the ENSO mode and a red spectrum for the PDO mode. In the SP-CCSM (Fig. 9c), the ENSO mode has a broad-band spectrum with a peak at 36 months while the PDO mode shows a red spectrum. Although the period of the ENSO mode in both CT-CCSM and SP-CCSM is lower than the observed period, the SP-CCSM is closer. In both model simulations, the period of the ENSO mode over South America is consistent with the period of the ENSO mode in SST (Stan et al. 2010) and in the South Asian monsoon (Krishnamurthy et al. 2013).

The spatial structure of the ENSO mode over South America is provided by the S-EOF1 of the corresponding RC. The ENSO mode in the observation (Fig. 10a) has an east–west dipole structure with negative (positive) anomalies over the equatorial Pacific and positive

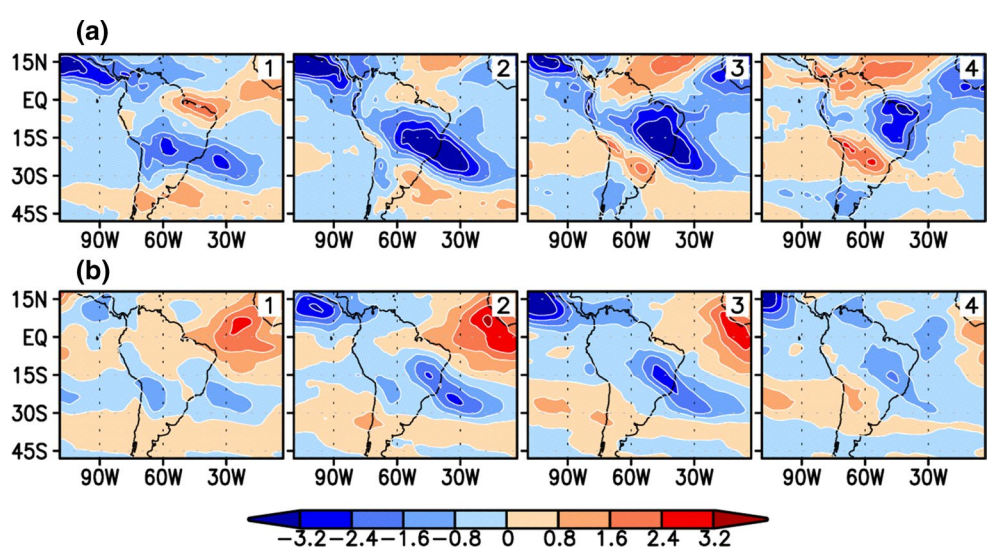

Fig. 7 Phase composites of the OLR RCs for four phase intervals of an average cycle of ISO in **a** observation and **b** SP-CCSM. The *phase number* is given at the *top right corner* of each panel. Units are in W m^{-2}

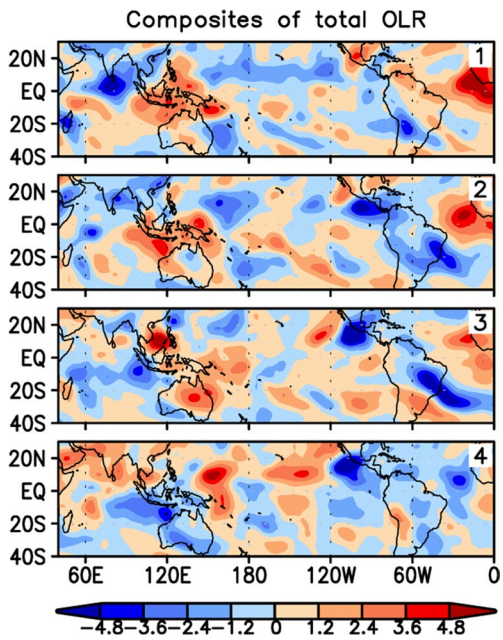

Fig. 8 Phase composites of total OLR anomalies for a half cycle of ISO in SP-CCSM. The *phase number* is given at the *top right corner* of each panel. Units are in W m^{-2}

(negative) anomalies over the northern part of the continent and the equatorial Atlantic. A north–south dipole structure separated at 20°S is also evident predominantly over the continent. The structure of the observed ENSO mode is fairly well captured by both CT-CCSM (Fig. 10b) and SP-CCSM (Fig. 10c) although with some differences. In the CT-CCSM, the anomalies over the Pacific are weaker while they are stronger over the equatorial Atlantic. The anomalies in the north–south dipole over the continent are slightly weaker in SP-CCSM whereas the anomalies over the equatorial Pacific and Atlantic oceans are better simulated. Overall, the spatial structure of the ENSO mode is better simulated in SP-CCSM than in CT-CCSM.

The spatial structure of the PDO mode is also shown in Fig. 10 by plotting the S-EOF1 of the corresponding RC. In the observation, the PDO mode consists of anomalies of one sign over much of the continent south of 10°S, south Pacific and much of the Atlantic south of the equator while anomalies of opposite sign exist over the northern continent and equatorial Pacific and Atlantic oceans (Fig. 10d). The PDO mode in the CT-CCSM (Fig. 10e) displays anomalies of same sign over most of the continent which extend into the equatorial Pacific with higher magnitude and anomalies of opposite sign appearing mainly in the subtropical Pacific. The PDO mode in the SP-CCSM (Fig. 10f) has better correspondence with the observed structure (Fig. 10d). The SP-CCSM captures the negative anomalies in the southern part although it does not extend up to 10°S over the eastern part of the continent. The positive anomalies

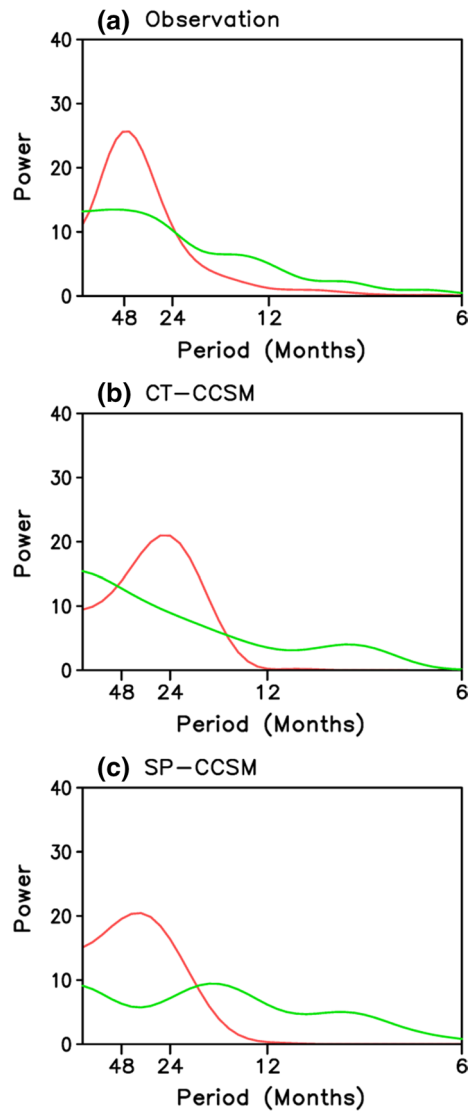

Fig. 9 Power spectra (month^{-1}) of the S-PC1 of the RCs of ENSO mode (*red*) and PDO mode (*green*) in **a** observation, **b** CT-CCSM and **c** SP-CCSM

cover the northern part of the continent but extend strongly over the equatorial Pacific.

5.2 Relation with SST

The discussion of the low-frequency modes so far has revealed that the SP-CCSM shows better representation of the ENSO and PDO modes compared to CT-CCSM although both the models have the same oceanic component. The introduction of superparameterization seems to have influenced the ocean–atmosphere interaction in the coupled model. The relation between the low-frequency atmospheric modes and SST is studied by computing the simultaneous point correlation of S-PC1 of the RC of each mode with the daily SST anomalies.

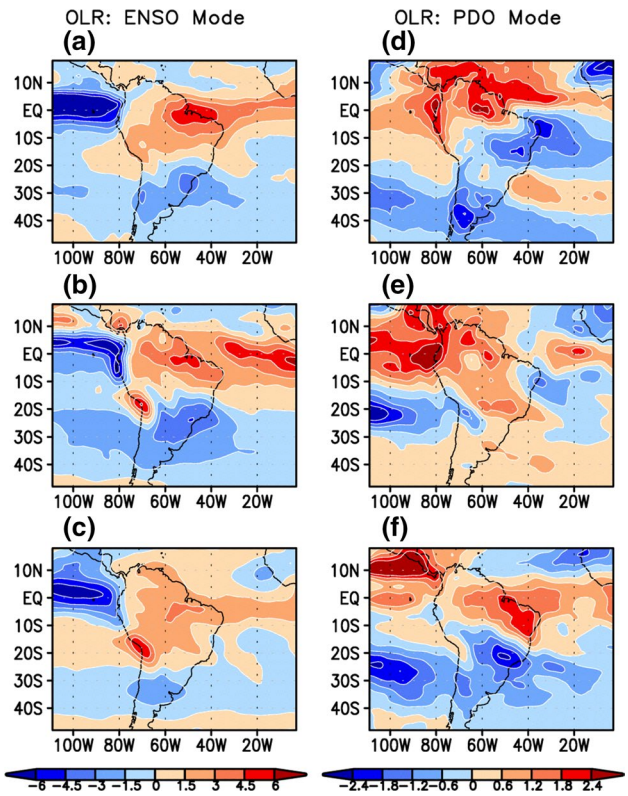

Fig. 10 Spatial EOF1 of the RC of ENSO mode in **a** observation, **b** CT-CCSM and **c** SP-CCSM. Spatial EOF1 of the RC of PDO mode in **d** observation, **e** CT-CCSM and **f** SP-CCSM. The Spatial EOF analysis was performed on the daily values of the RCs. Units are in W m^{-2}

The correlation of the ENSO mode with the SST in the observation (Fig. 11a) clearly shows the ENSO signature with strong positive correlation in the equatorial eastern and central Pacific surrounded by the horseshoe-shaped moderate negative correlation in the Pacific and weaker positive correlation in the Indian Ocean. In the model correlation of the ENSO, the SP-CCSM (11c) seems to capture the observed structure better than the CT-CCSM (Fig. 11b). In the CT-CCSM, stronger positive correlation extends too far to the west in a narrower belt along the equator. The positive correlation in the SP-CCSM is comparable to the observed structure in the equatorial Pacific although weaker correlation extends further west. The negative correlation in the Pacific and the positive correlation in the Indian ocean are also better captured by the SP-CCSM.

For the PDO mode in the observation, the correlation with the SST shows negative correlation in a large region of the northern Pacific accompanied by positive correlation along the west coast of North America and central Pacific, consistent with the SST pattern associated with the PDO (Mantua et al. 1997). The correlation pattern of the PDO mode in the CT-CCSM (Fig. 11e) consists of positive correlations over almost the entire domain except for small regions of negative correlation in the North Pacific and the Atlantic and has little correspondence with he observed structure. The correlation of the PDO mode in the SP-CCSM (Fig. 10f) shows fairly good correspondence with the observed structure in all the ocean basins. However, there are some differences in the detailed structure of the correlation pattern in the northern Pacific.

5.3 Interannual variability

Based on observations and model experiments, Charney and Shukla (1981) hypothesized that the interannual variability of the tropical climate is mainly determined by the slowly varying boundary conditions such as SST, soil moisture and snow cover. This hypothesis was supported by studies on the South Asian monsoon (Krishnamurthy and Shukla 2007, 2008) which further showed that high-frequency variability such as the intraseasonal oscillations do not contribute significantly to the interannual variability of the seasonal mean monsoon. Krishnamurthy and Misra (2011) demonstrated that the SST-related atmospheric modes mainly determine the interannual variability over South America also. In this section, the ability of the CT-CCSM and SP-CCSM in determining the interannual variability in the South American climate through the ENSO and PDO modes is discussed.

The interannual variability over South America also shows regional variations (Krishnamurthy and Misra 2011). To show the regional difference, domains in the Amazon River Basin (ARB) and central-east South America (CESA) are considered, following Krishnamurthy and Misra (2011). The ARB and CESA domains are (70°W–50°W, 5°S–5°N) and (60°W–40°W, 20°S–10°S), respectively. The area averages over these domains will be referred to as ARB and CESA indices. The ARB and CESA indices are plotted in Fig. 12 by computing the area averages of the daily RCs of the ENSO and PDO modes in observation, CT-CCSM and SP-CCSM. Although all the time series plotted in Fig. 12 are daily values, the ENSO and PDO modes clearly reveal low-frequency variability.

The ARB and CESA indices of the ENSO mode in the observation (Fig. 12a) have captured the major ENSO events. Although both ARB and CESA indices are in phase, the ARB index has higher values during the ENSO events, indicating stronger influence of the Pacific over the northern part of the continent. In the CT-CCSM (Fig. 12b), the variability of the ARB and CESA indices of the ENSO mode is more regular and biennial, consistent with the power spectrum shown earlier (Fig. 9b). The ARB and CESA indices are also almost out of phase. The ARB and CESA indices of the ENSO mode in SP-CCSM (Fig. 12c) have more chaotic variation with longer time

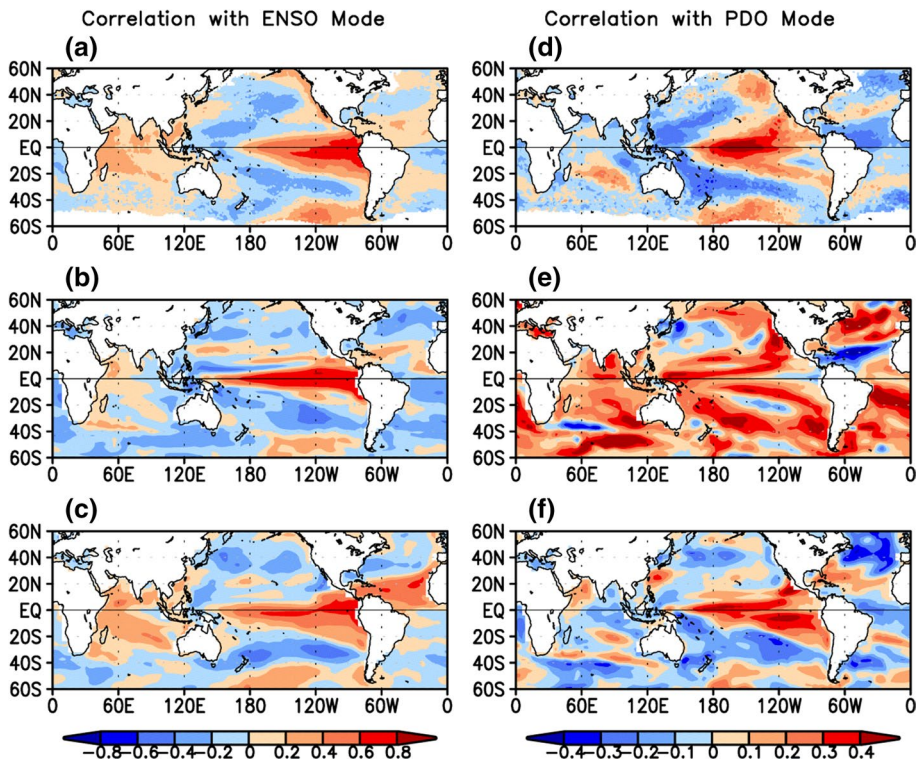

Fig. 11 Simultaneous point correlation of daily S-PC1 of ENSO mode with daily SST anomalies in **a** observation, **b** CT-CCSM and **c** SP-CCSM. Simultaneous point correlation of daily S-PC1 of PDO mode with daily SST anomalies in **d** observation, **e** CT-CCSM and **f** SP-CCSM. The PCs correspond to the EOFs shown in Fig. 10

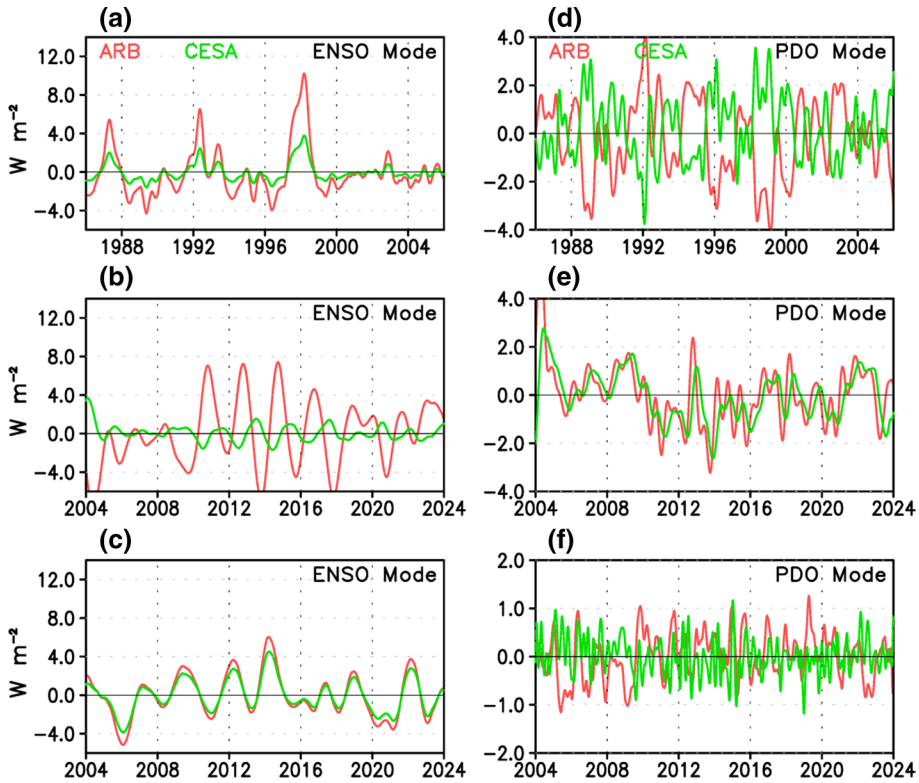

Fig. 12 Daily time series of ARB index (*red*) and CESA index (*green*) of RC of ENSO mode in **a** observation, **b** CT-CCSM and **c** SP-CCSM. Daily time series of ARB index (*red*) and CESA index (*green*) of RC of PDO mode in **d** observation, **e** CT-CCSM and **f** SP-CCSM. Note that the scale of y-axis in **f** is different from **d** and **e**

scale, comparable to the observed variability. The ARB and CESA indices in SP-CCSM vary in-phase although their magnitudes are almost equal. The peaks corresponding to ENSO events occur during the austral summer season in the observation. A closer examination has revealed that SP-CCSM also has ENSO peaks occurring during austral

summer, as in observation, while the CT-CCSM shows peaks occurring earlier than the austral summer. Thus, the SP-CCSM shows better simulation of the observed interannual variability and regional variation of the ENSO mode compared to CT-CCSM. Stan et al. (2010) noted that ENSO by itself is better simulated in SP-CCSM3 and attributed the improvement in the period and irregularity of ENSO to the better representation of cloud-scale processes in the atmospheric model, which in turn may provide proper ocean–atmosphere interaction in the ENSO region. Further, the improved simulation of the MJO may also be partially responsible for the better ENSO simulation. The atmospheric ENSO mode over South America may be considered as the response to the better simulation of ENSO mode over the Pacific.

In the PDO mode of the observation, the ARB and CESA indices vary with opposite phase but with almost equal magnitude (Fig. 12d). The PDO mode can modulate the interannual variability due to ENSO. In the CT-CCSM, the ARB and CESA indices of the PDO mode (Fig. 12e) are varying in-phase with almost equal amplitude, reflecting the spatial pattern of this mode (Fig. 10e). The variations of ARB and CESA indices of the PDO mode in the SP-CCSM resemble those of the observation with out-of-phase relation between the indices. The magnitude of the PDO mode in SP-CCSM, however, is about half of the observed magnitude.

6 Summary and discussion

In this study, the simulation of the climate over South America by a coupled ocean–atmosphere model which includes embedded cloud resolving models was examined. In particular, the NCAR CCSM model was used to test the ability of the superparameterized version to simulate the observed seasonal and intraseasonal oscillations and the low-frequency modes in the South American climate. A comparison with the simulation by the CCSM with conventional parameterization of convection was carried out to test whether the explicit treatment of convection and cloud processes in SP-CCSM improves the simulation of convection and also large-scale processes over South America. The main results indicate that SP-CCSM is better than CT-CCSM in simulating the leading seasonal and intraseasonal oscillations and the ENSO and PDO modes.

The analysis of the observation and model simulations followed the same approach of Krishnamurthy and Misra (2011) to extract different modes of variability of the South American climate. For this purpose, the data-adaptive method of MSSA was employed on raw anomalies without requiring pre-filtering or any assumptions about the time scales of the extracted modes. The CT-CCSM was able to simulate only the seasonal oscillation while the SP-CCSM was successful in simulating both the seasonal and intraseasonal oscillations. Although both models showed some disagreement with the observation in the period of the SO, the spatial structure and the northeastward propagation of the SO were better simulated by the SP-CCSM compared to CT-CCSM. The relation between SO and NAO was also better captured by the SP-CCSM. The ISO was simulated only by the SP-CCSM with a period closer to that of observation. The spatial structure and the northeastward propagation of the ISO and its association with the MJO were reasonably well simulated by the SP-CCSM when compared to observation.

Both CT-CCSM and SP-CCSM were able to simulate two leading observed low-frequency modes. The two models were successful in simulating the ENSO and PDO modes but with differences. However, either model was unable to resolve the AMO mode found in the observation by Krishnamurthy and Misra (2011). While the CT-CCSM generated more regular variability at biennial time scale in the ENSO mode, the SP-CCSM was able to simulate more irregular variability of the ENSO mode with a time scale closer to that in the observation. The spatial structure, relation with the Pacific SST and the regional variation were also better simulated in the SP-CCSM than in CT-CCSM. The spatial structure of the PDO mode in the SP-CCSM was closer to the observed pattern while the PDO mode in the CT-CCSM showed considerable difference. The observed relation between the PDO mode and the Pacific SST was well captured by the SP-CCSM whereas the CT-CCSM showed completely different pattern. The interannual variability of the PDO mode in SP-CCSM showed the observed phase relation between ARB and CESA while the CT-CCSM showed in-phase relation. However, the magnitude of the PDO mode was lower in the SP-CCSM compared to observation.

This study has provided further support to the importance of realistic cloud parameterization and the necessity of coupled models. The better performance of the SP-CCSM over South America adds to the success of the superparameterization that was also seen in the simulation of the South Asian monsoon (Krishnamurthy et al. 2013). Some of the shortcomings in the simulation of the oscillations by the SP-CCSM, such as the difference in the period and spatial structure, need further investigation. In the low-frequency modes, the absence of the AMO mode and the lower magnitude of the PDO mode require further study.

Acknowledgments This research was supported by Grants from the National Science Foundation (ATM-0830068, AGS-1211848), the National Oceanic and Atmospheric Administration (NA09OAR4310058), and the National Aeronautics and Space Administration (NNX09AN50G). The authors acknowledge the support of the Computational and Information Systems Laboratory at NCAR for providing computer time for this work.

References

Aceituno P (1988) On the functioning of the Southern oscillation in the South American sector Part I: surface climate. Mon Weather Rev 116:505–524

Bombardi RJ, Carvalho LMV (2009) IPCC global coupled climate model simulations of the South American monsoon system. Clim Dyn 33:893–916

Carvalho LMV, Jones C, Liebmann B (2002a) Extreme precipitation events in southeastern South America and large-scale convective patterns in the South Atlantic convergence zone. J Clim 15:2377–2394

Carvalho LMV, Jones C, Silva Dias MAF (2002b) Intraseasonal large-scale circulations and mesoscale convective activity in tropical South America during the TRMM-LBA campaign. J Geophys Res 107:D20. doi:10.1029/2001JD000745

Carvalho LMV, Jones C, Liebmann B (2004) The South Atlantic convergence zone: intensity, form, persistence, and relationships with intraseasonal to interannual activity and extreme rainfall. J Clim 17:88–108

Charney JG, Shukla J (1981) Predictability of monsoons. In: Lighthill J, Pearce RP (eds) Monsoon dynamics. Cambridge University Press, Cambridge, pp 99–109

Collins WD et al (2006) The Community Climate System Model version 3 (CCSM3). J Clim 19:2122–2143

Dee DP et al (2011) The ERA-Interim re-analysis: configuration and performance of the data assimilation system. Quart J R Meteorol Soc 137:553–597

DeMott CA, Stan C, Randall DA, Kinter JL III, Khairoutdinov M (2011) The Asian monsoon in the superparameterized CCSM and its relationship to tropical wave activity. J Clim 24:5134–5156

DeMott CA, Stan C, Randall DA (2013) Northward propagation mechanisms of the boreal summer intraseasonal oscillation in the ERA-Interim and SP-CCSM. J Clim 26:1973–1992

Fu R, Chen M, Li W, Dickinson RE (2001) How do tropical sea surface temperatures influence the seasonal distribution of precipitation in the equatorial Amazon? J Clim 14:4003–4026

Ghil M, Allen MR, Dettinger MD, Ide K, Kondrashov KD, Mann ME, Robertson AW, Saunders A, Tian Y, Varadi F, Yiou P (2002) Advanced spectral methods for climatic time series. Rev Geophys 40(1):1003. doi:10.1029/2000RG000092

Grabowski WW (2001) Coupling cloud processes with the large-scale dynamics using the cloud-resolving convection parameterization (CRCP). J Atmos Sci 58:978–997

Grimm AM, Vera C, Mechoso CR (2005) The South American monsoon system. In: The global monsoon system: research and forecast. World Meteorological Organization, Geneva. WMO/TD No. 1266:219–238

Guilyardi E, Wittenberg A, Fedorov A, Collins M, Wang C, Capotondi A, van Oldenborgh GJ, Stockdale T (2009) Understanding El Niño in ocean-atmosphere general circulation models: progress and challenges. Bull Am Meteorol Soc 90:325–340

Jones C, Carvalho LMV (2002) Active and break phases in the South American monsoon system. J Clim 15:905–914

Khairoutdinov M, Randall DA (2001) A cloud resolving model as a cloud parameterization in the NCAR Community Climate System Model: preliminary results. Geophys Res Lett 28:3617–3620

Khairoutdinov M, Randall DA (2003) Cloud-resolving modeling of ARM summer 1997 IOP: model formulation, results, uncertainties and sensitivities. J Atmos Sci 60:607–625

Kousky VE, Kagano MT, Cavalcanti IFA (1984) A review of the Southern oscillation: ocean-atmospheric circulation changes and related rainfall anomalies. Tellus 36A:490–504

Krishnamurthy V, Misra V (2010) Observed teleconnections with the South American monsoon system. Atmos Sci Lett 11:7–12

Krishnamurthy V, Misra V (2011) Daily atmospheric variability in the South American monsoon system. Clim Dyn 37:803–819

Krishnamurthy V, Shukla J (2007) Intraseasonal and seasonally persisting patterns of Indian monsoon rainfall. J Clim 20:3–20

Krishnamurthy V, Shukla J (2008) Seasonal persistence and propagation of intraseasonal patterns over the Indian monsoon region. Clim Dyn 30:353–369

Krishnamurthy V, Stan C, Randall DA, Shukla RP, Kinter JL III (2013) Simulation of the South Asian monsoon in a coupled model with an embedded cloud resolving model. J Clim. doi:10.1175/JCLI-D-13-00257.1

Lenters JD, Cook KH (1997) On the origin of the Bolivian high and related circulation features of the South American climate. J Atmos Sci 54:656–678

Liebmann B, Smith CA (1996) Description of a complete (interpolated) outgoing longwave radiation dataset. Bull Am Soc 77:1275–1277

Liebmann B, Kiladis GN, Marengo JA, Ambrizzi T, Glick JD (1999) Submonthly convective variability over South America and the South Atlantic convergence zone. J Clim 12:1877–1891

Liebmann B, Jones C, Carvalho LMV (2001) Interannual variability of daily extreme precipitation events in the state of SO Paulo, Brazil. J Clim 14:208–217

Liebmann B, Marengo JA, Vera CS, Saulo AC (2004) Subseasonal variations of rainfall in South America in the vicinity of the low-level jet east of the Andes and comparison to those in the South Atlantic convergence zone. J Clim 17:3829–3842

Lin J-L et al (2006) Tropical intraseasonal variability in 14 IPCC AR4 climate models. Part I: convective signals. J Clim 19:2665–2690

Madden RA, Julian PR (1994) Observations of the 40–50-day tropical oscillation–a review. Mon Weather Rev 122:814–837

Mantua NJ, Hare SR, Zhang Y, Wallace JM, Francis RC (1997) A Pacific decadal climate oscillation with impacts on salmon production. Bull Am Meteorol Soc 78:1069–1079

Marengo JA (1992) Interannual variability of surface climate in the Amazon Basin. Int J Climatol 12:853–863

Marengo JA (1995) Interannual variability of deep convection over the tropical South American sector as deuced from ISCCP C2 data. Int J Climatol 15:995–1010

Marengo JA et al (2012) Recent developments of the South American monsoon system. Int J Climatol 32:1–21

Misra V (2008a) Coupled air sea and land interactions of the South American monsoon. J Clim 21:6389–6403

Misra V (2008b) Coupled interactions of the monsoons. Geophys Res Lett 35:L12705. doi:10.1029/2008GL033562

Moron V, Vautard R, Ghil M (1998) Trends, interdecadal and interannual oscillations in global sea-surface temperatures. Clim Dyn 14:545–569

Nogués-Paegle J, Mo KC (1997) Alternating wet and dry conditions over South America during summer. Mon Weather Rev 125:279–291

Nogués-Paegle J et al (2002) Progress in Pan American CLIVAR research: understanding the South American monsoon. Meteorologica 27:3–30

Plaut G, Vautard R (1994) Spells of low-frequency oscillations and weather regimes in the Northern hemisphere. J Atmos Sci 51:210–236

Randall DA et al (2007) Climate models and their evaluation. In: Solomon S et al (eds) Climate change 2007: the physical science basis. Contribution of working group I to the fourth assessment report of the intergovernmental panel on climate change. Cambridge University Press, Cambridge, pp 589–662

Rao VB, Cavalcanti I, Hada K (1996) Annual variation of rainfall over Brazil and water vapor characteristics over South America. J Geophys Res 101:26359–26551

Reynolds RW, Smith TM, Liu C, Chelton DB, Casey KS, Schlax MG (2007) Daily high-resolution-blended analyses for sea surface temperature. J Clim 20:5473–5496

Ropelewski CF, Halpert MS (1987) Global and regional scale precipitation patterns associated with the El Niño/Southern oscillation. Mon Weather Rev 115:1606–1626

Silva GAM, Ambrizzi T (2006) Inter-El Niño variability and its impact on the South American low-level jet east of the Andes during austral summer—two case studies. Adv Geosci 6:283–287

Silva GAM, Ambrizzi T, Marengo JA (2009) Observational evidences on the modulation of the South American low level jet east of the Andes according the ENSO variability. Ann Geophys 27:645–657

Silva GAM, Drumond A, Ambrizzi T (2011) The impact of El Niño on South American summer climate during different phases of the Pacific decadal oscillation. Theor Appl Climatol 106:307–319

Stan C, Khairoutdinov M, DeMott CA, Krishnamurthy V, Straus DM, Randall DA, Kinter JL III, Shukla J (2010) An ocean-atmosphere climate simulation with an embedded cloud resolving model. Geophys Res Lett 37:L01702. doi:10.1029/2009GL040822

Vera C et al (2006) Toward a unified view of the American monsoon systems. J Clim 19:4977–5000

Zhang GJ, McFarlane NA (1995) Sensitivity of climate simulations to the parameterization of cumulus convection in the Canadian climate centre general circulation model. Atmos Ocean 33:407–446

Zhou J, Lau K-M (1998) Does a monsoon climate exist over South America? J Clim 11:1020–1040